Biointerphases (2012) 7:24
DOI 10.1007/s13758-012-0024-z

ARTICLE

Comparison Between Empirical Protein Force Fields for the Simulation of the Adsorption Behavior of Structured LK Peptides on Functionalized Surfaces

Galen Collier · Nadeem A. Vellore · Jeremy A. Yancey · Steven J. Stuart · Robert A. Latour

Received: 13 January 2012 / Accepted: 17 February 2012 / Published online: 1 March 2012

Abstract All-atom empirical molecular mechanics protein force fields, which have been developed to represent the energetics of peptide folding behavior in aqueous solution, have not been parameterized for protein interactions with solid material surfaces. As a result, their applicability for representing the adsorption behavior of proteins with functionalized material surfaces should not be assumed. To address this issue, we conducted replica-exchange molecular dynamics simulations of the adsorption behavior of structured peptides to functionalized surfaces using three protein force fields that are widely used for the simulation of peptide adsorption behavior: CHARMM22, AMBER94, and OPLS-AA. Simulation results for peptide structure both in solution and when adsorbed to the surfaces were compared to experimental results for similar peptide-surface systems to provide a means of evaluating and comparing the performance of these three force fields for this type of application. Substantial differences in both solution and adsorbed peptide conformations were found amongst these three force fields, with the CHARMM22 force field found to most closely match experimental results.

Electronic supplementary material The online version of this article (doi:10.1007/s13758-012-0024-z) contains supplementary material, which is available to authorized users.

G. Collier · N. A. Vellore · J. A. Yancey · R. A. Latour (✉)
Department of Bioengineering,
Clemson University, Clemson, SC 29634, USA
e-mail: latourr@clemson.edu

S. J. Stuart
Department of Chemistry, Clemson University,
Clemson, SC 29634, USA

1 Introduction

The study of interfacial phenomena in biological systems, such as peptide-surface and protein-surface interactions, often requires the analysis of mechanistic processes at the atomic level that are not easily determined using experimental techniques. Molecular simulation provides a complementary approach to study these types of interactions that enables the spatial and temporal features of such complex molecular mechanisms to be directly predicted and visualized.

Empirical all-atom molecular mechanics force fields (FFs) are typically used for the simulation of molecular systems that are too large to be efficiently studied using quantum mechanical simulation methods. Due to their unique analytical capabilities, FF-based simulations have the potential to provide highly accurate representations of biological systems and phenomena. However, most empirical all-atom molecular mechanics FFs that have been used to represent the interactions between biomolecules, such as peptides and proteins, with material surfaces have been developed and parameterized specifically for the simulation of biomolecules in aqueous solution without considering adsorption behavior. Since FFs such as these are empirically parameterized for specific applications, a given set of FF parameters that are tuned for one application (i.e., within some particular molecular environment) may not be suitable for a different application. This issue is referred to as FF transferability [1]. Limitations in the transferability of a FF can inhibit its usefulness in simulations of novel systems where the types of atomic interactions being represented extend beyond those for which that FF was developed. A clear example of this problem has been demonstrated by van Gunsteren and coworkers [2], where they showed that different sets of partial charge parameters were needed for

the GROMOS96 FF [3] to accurately represent a set of molecules in their pure liquid state compared to when they were represented in aqueous solution.

FF transferability is a significant issue in the simulation of interfacial phenomena and especially in the simulation of peptide and protein adsorption to synthetic material surfaces. Simulations of peptide and protein adsorption behavior are typically performed using protein FFs such as the CHARMM22 [4], AMBER94 [5], and OPLS-AA [6] FFs, which have been parameterized, tuned, and validated to represent peptide structure and energetics in aqueous solution. The transferability of these FFs to simulations of peptide and protein adsorption is questionable because of differences in the primary driving forces that govern peptide conformational behavior in aqueous solution compared to those that mediate adsorption behavior at a liquid–solid interface. In aqueous solution, peptide conformational behavior is heavily influenced by the bonded parameters of a FF (e.g., dihedral angle rotation) while peptide adsorption behavior is dominated by nonbonded interaction parameters (e.g., van der Waals and electrostatic interactions). Additionally, the subtle balance between the relative attractions of a peptide versus water molecules for functional groups presented by an adsorptive surface plays a very important role in the adsorption process, with small imbalances in their nonbonded parameters potentially resulting in large errors in simulated adsorption behavior.

One of the difficulties in addressing these concerns is the limited amount of quantitative experimental data that is available on the orientation and conformation of adsorbed peptides from which simulation results using a given FF can be quantitatively assessed. An experimental study by DeGrado and Lear [7] provides an excellent example of the kind of data that can be used for such comparisons in which the orientation and conformation of small structured peptides composed of sequences of leucine–lysine (LK) amino acids residues were determined in aqueous solution and when forming a monolayer at the air/water interface (emulating a hydrophobic surface) and on both polar and nonpolar material surfaces. The peptides used in these studies serve as excellent model structures because they adopt specific and varying secondary structure conformations and molecular orientations depending on the surfaces with which they come in contact. Recently, a larger set of experimental studies has been published by Phillips and coworkers [8] on the adsorption behavior of this same set of LK peptides to both hydrophobic polystyrene and hydrophilic silica surfaces. Additionally and most recently, Castner and coworkers [9–12] have completed a comprehensive set of experiments studying the conformations and orientations of similar LK peptides adsorbed to a variety of material surfaces, including a hydrophobic methyl-terminated self-assembled monolayer (SAM) surface and a negatively charged carboxylic acid-terminated SAM on a gold substrate. The peptide-SAM surface studies completed by Castner and coworkers, coupled with results from similar previous studies, provide an excellent opportunity for the evaluation of different FFs in order to determine which FF is most capable of accurately representing peptide adsorption behavior for these types of systems.

The objective of the work presented in this paper was to conduct molecular dynamics (MD) simulations of the adsorption behavior of structured LK peptides to surface chemistries matching those used in the experimental studies described above, using the three FFs that are most widely used for the simulation of peptide and protein adsorption behavior (i.e., CHARMM22, AMBER94, and OPLS-AA FFs). The simulation results for each FF were compared to the available experimental results and this information was used as a basis to evaluate the transferability of each of these FFs to accurately represent peptide adsorption behavior for these systems.

2 Methods

2.1 Model Molecular Systems

DeGrado and Lear [7] introduced LK peptides, which are short peptides composed exclusively of leucine (L) and lysine (K) amino acid residues sequentially arranged to represent specific secondary structural elements that are found in proteins. Two of the peptides they introduced, a 7-mer β-strand-forming LK sequence (LKβ7; LKLKLKL) and a 14-mer α-helix-forming LK sequence (LKα14; LKKLLKLLKKLLKL), served as the model peptides used in our simulations. When these peptides adopt β-strand and α-helical conformations, respectively, the leucine side chains lie on one side of the peptide backbone while the lysine residue side chains lie on the other side (Fig. 1). This arrangement results in amphiphilic peptides that have both a hydrophobic side and a positively charged hydrophilic side, thus causing them to orient in a predictable fashion as they adsorb to either hydrophobic or negatively charged surfaces.

For our simulations, the same set of LK peptides used by DeGrado and Lear was constructed using parameters from the CHARMM22 (with CMAP [13]), AMBER94, and OPLS-AA FFs. Similar to the experimental studies, each peptide was terminated via N-terminal acetylation and C-terminal amidation (ACE and CT2 residues, respectively). For the LKβ7 simulations, a pair of identical LKβ7 peptides was used to allow the formation of both parallel and antiparallel β-sheets. Simulations of LKα14 used a single peptide. Each system was composed of the peptide(s) alone in an aqueous solution composed of explicitly

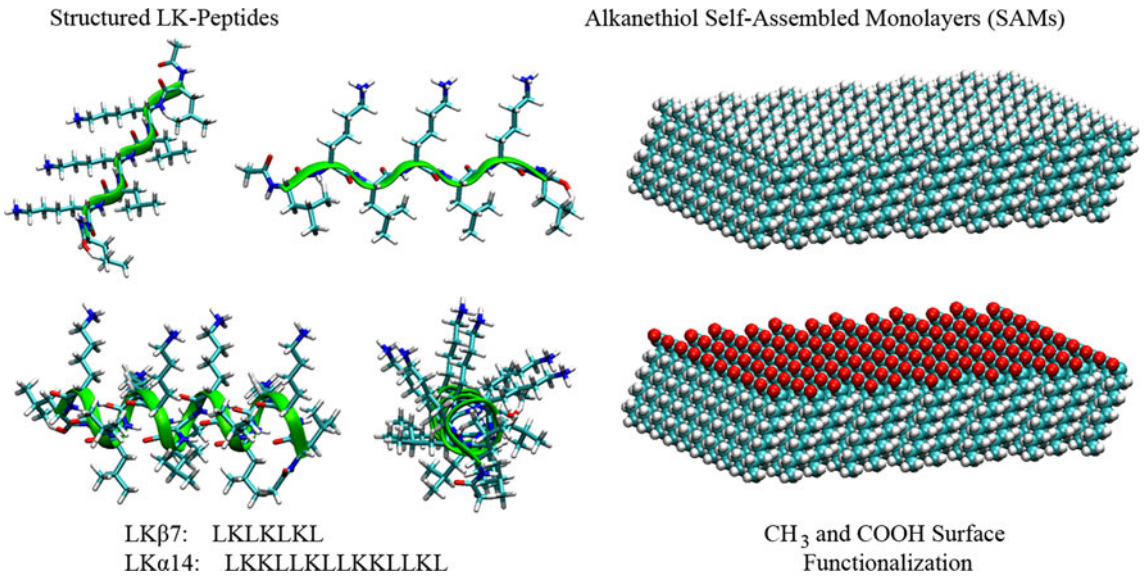

Fig. 1 Images representing the LK-peptides and the functionalized SAM surfaces. The LKβ7 peptide is shown, *upper left*, from the *end* and from the *side*. The LKα14 peptide is shown, *lower left*, from the *side* and from the *end*. The CH_3-SAM is shown, *upper right*, and the COOH-SAM is shown, *lower right*

represented TIP3P water with 140 mM Na^+ and Cl^- ions added to represent physiological saline conditions, or in 140 mM saline solution over a functionalized alkanethiol SAM surface, with additional Cl^- counter-ions added to neutralize the positively charged K side chains.

The model surfaces used in these studies were representations of defect-free, idealized SAM surfaces comprised of alkyl chains with functionalized terminal groups (Fig. 1). In these surfaces, the alkyl chains form a tightly packed structure in which the chains were arranged in $\left(\sqrt{3} \times \sqrt{3}\right)R3^\circ$ geometry with 5 Å spacing, with the chains tilted initially to the orientation specified by Vericat and coworkers [14] at approximately 30° from the surface normal, thus representing alkanethiol SAMs formed on a gold substrate [15]. The two SAM surfaces used in this study were represented by a hydrophobic, methyl-terminated SAM (CH_3-SAM) and a hydrophilic, negatively charged carboxylic acid-terminated SAM (COOH-SAM). These surfaces were constructed using methods that Latour and coworkers [16–22] and others [23–28] have used in several previous simulation studies involving SAMs. The SAM surfaces were each represented as consisting of functionalized alkyl chains of 10 carbons, including the functional group carbon. 50% of the carboxylic acid groups of the COOH-SAM were deprotonated, as appropriate for the experimentally determined pK_a value of 7.4 [22]. To maintain neutrality of the systems with the COOH-SAM, 60 additional Na^+ counter-ions were included in the simulated water box for neutralization of the 60 surface charges.

The functionalized alkyl residues that make up each SAM surface were lacking FF parameters in some of the FFs. These missing FF parameters were obtained by assigning partial charges and atom types matching those of similar atomic arrangements existing within corresponding amino acid side chain functional groups from each respective FF. The terminal carboxylate and carboxylic acid functional group parameters for the COOH-SAM were assigned based on the side-chain parameters for deprotonated glutamic acid and protonated glutamic acid residues, respectively. The terminal CH_3 group parameters for the CH_3-SAM were assigned based on the alanine (ALA) residue side chain in each FF.

2.2 Simulation Details

The construction of all of the molecular structures and the simulation of all of the systems were accomplished using the standard CHARMM (version c34b2) suite of simulation tools [29]. All structural components of each system were developed using incremental equilibration stages using the same FF that would be used for the simulations conducted with the same systems. The specific parameter and topology files that constitute the CHARMM22, AMBER94, and OPLS-AA FFs were the ones included with the CHARMM c34b2 source package, plus the addition of Cl^- and Na^+ ion Lennard-Jones parameters converted for use with the CHARMM simulation program from the original OPLS-AA FF.

Each peptide-surface model system comprised an orthorhombic layer of mobile water molecules, ions, and peptides bounded above by a fixed bulk water layer and below by a fixed SAM surface with unrestrained functional

groups (Fig. 2). We refer to the central layer of mobile water molecules, ions, and peptides as the mobile core, and for spatial reference purposes, we consider the positive z axis as the axis directed normal to the SAM surface, directed toward the solution phase. All systems were simulated using 3-D periodic boundary conditions (PBCs) using the explicit-image model. The particle-mesh Ewald (PME) method [30] was used for calculation of long-range electrostatics. Parameterization of PME [31] for all simulations included truncation of the real-space summation at 12 Å, a value of 0.34 $Å^{-1}$ for the Ewald method's Gaussian distribution inverse width, and a real-space cutoff of 12 Å. Van der Waals (vdW) interactions were truncated using a force-based switching function at cutoff distances matching those of the PME parameterization. All simulations were conducted in the canonical (NVT) ensemble using the VV2 integrator (an implementation of the velocity Verlet algorithm [32]). The Nosé-Hoover method [33] with a thermostat time constant of 0.1 ps was used for temperature control of all replicas. Bond lengths involving heavy atoms and hydrogens (X–H bonds) were held fixed using the SHAKE algorithm [34], which enabled a 2.0 fs time step to be used for all equilibration and production dynamics.

The mobile core of all simulated peptide-surface systems was constructed beginning with a 50 × 52 × 41 $Å^3$ volume containing 3,400 TIP3P waters with 8 Na^+ ± and 8 Cl^- ions sufficient to provide an approximately 140 mM NaCl aqueous solution (i.e., physiological saline), and this saline system was equilibrated for over 1 ns at 298 K. After equilibration, peptides and additional ions sufficient for neutralizing each peptide and the COOH-SAM surface were added to this saline system. Water molecules whose O or H atoms were within 2.1 Å of any non-hydrogen peptide atom were removed, and ions were added by replacing TIP3P waters with the added ions. Each of these mobile core systems containing a peptide (or pair of peptides) was again equilibrated for 1 ns and the volume was adjusted so that it produced an average pressure of 1 atm. Finally, the mobile core was placed between the fixed bulk water layer and the SAM surface and the positions of those layers were adjusted so that a 1 ns equilibration of the complete system could be conducted with the mobile core maintaining its average volume as estimated from the density of solution near the interface (virial-based pressure measurements were not used in this stage of complete system equilibration, as they are unreliable in systems with constrained atoms) [35]. The 15 Å thick fixed bulk water layer at the top of the mobile core, containing 3 Na^+ and 3 Cl^- ions within TIP3P water, was equilibrated at 298 K before being constrained. All atoms of this layer were held fixed during the production simulations so that the free water molecules of the mobile core would interface with a bulk solution-like surface instead of the periodic image of the hydrophobic bottom of the SAM's alkyl chains. The alkyl chains of the SAMs were also held fixed during the simulations, but the terminal alkyl carbons and all surface functional group atoms were unrestrained. The peptide-solution systems were constructed similarly, but without the SAM or rigid water layers. Overall, two distinct systems (one solo LKα14 and one pair of LKβ7s) were constructed and simulated as aqueous solutions with no SAM surface present, and four distinct systems were constructed and simulated with a SAM surface: one LKα14 and a pair of LKβ7s were each simulated in the presence of each of the SAMs.

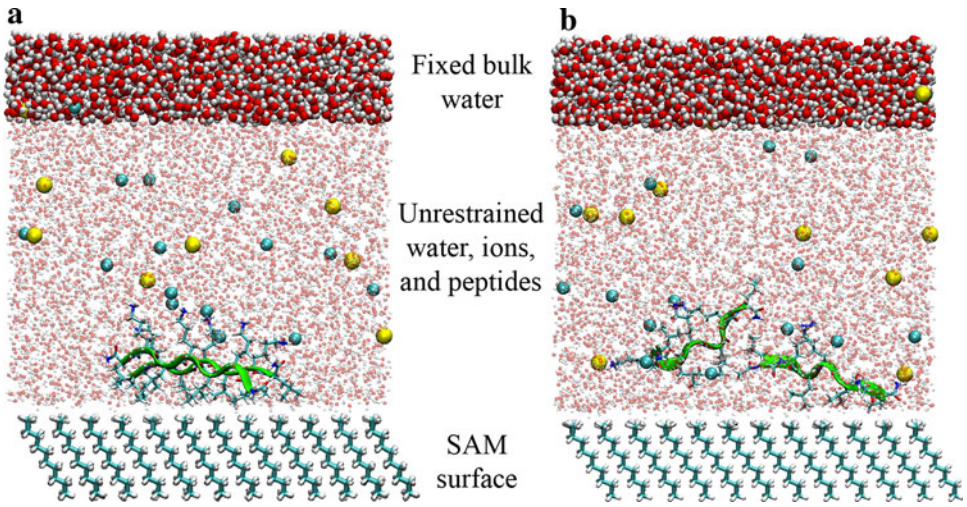

Fig. 2 Diagrams of one of the simulated systems, the pair of LKβ7 peptides adsorbed to the CH_3-SAM surface. Both images were generated from single trajectory frames of the production-phase REMD simulations using **a** the CHARMM22 FF and **b** the OPLS-AA FF. Freely diffusing Na^+ (*yellow*) and Cl^- (*cyan*) ions are also present in the solution above each SAM surface. In these images, the differences in the conformations and orientations of the 2 LKβ7 peptides highlight some of the differences between the FFs used for these simulations

In order to produce a large representative equilibrated ensemble of structures that could be analyzed to identify peptide structural trends for each system. The replica-exchange molecular dynamics (REMD) method introduced by Sugita and Okamoto [36] was used to maximize each system's exploration of conformational space. In the temperature-based implementation of the REMD method used here, as system configurations move from temperature level to temperature level (replica to replica) through the implementation of a Metropolis-like exchange process, conformational changes (i.e., crossing of potential energy barriers) that are more accessible at higher temperatures lead to the sampling of new low-energy states that subsequently migrate by exchange into the lower temperature levels, improving the sampling of states in the low-temperature levels. The resulting collection of states comprises a Boltzmann-weighted ensemble of equilibrated states for each system, as is necessary for proper comparison with experimental results.

The REMD simulation procedure for each system was coordinated using the MMTSB suite of simulation tools [37]. In order to enhance the sampling efficiency of the REMD simulations, the starting configurations for various REMD replicas were chosen from three different conformations of each peptide system. Each REMD simulation was comprised of 40 replicas spanning a temperature range of 298–520 K. Each REMD simulation was conducted with 1.0 ps MD intervals between exchange attempts and thorough equilibration prior to initiating the production REMD simulation. Immediately before each exchange attempt, the coordinates of the atoms of the 298 K replica were saved as a contribution to the overall low-temperature (298 K) ensemble of structures. Secondary structure analysis was conducted using the STRIDE [38] utility. Visualization software used during analysis of the simulation results included visual molecular dynamics (VMD) [39] and UCSF Chimera [40].

Since an REMD simulation includes replicas at elevated temperatures, a unique simulation problem for interfacial systems exists where the interaction of interest is between a mobile molecular species in solution (i.e., the peptide) and a surface with a fixed position. The possibility of the molecular species drifting away from the surface during the simulation, particularly for high-temperature replicas, must be addressed in order to maintain the simulated system in an arrangement that continually produces useful data (i.e., sampled states of the peptide interacting with the surface). Additionally, this modification must be done in a way that does not interfere with the interaction of interest. To accomplish this, a harmonic constraint potential was used to prevent the movement of a peptide away from the SAM surface. This potential force was applied to the center of mass of each peptide to avoid disruption of conformational characteristics, and it was only enabled if the center of mass of the peptide drifted beyond a distance of 10 Å from the topmost alkyl carbon atoms of each SAM surface. Monitoring of the activation of this potential force over the course of the simulations showed that it was enabled during less than 1% of all dynamics steps.

To provide an additional means of assessing the reproducibility of these complex simulations and to provide a measure of sampling convergence, each REMD simulation was conducted in duplicate, thus enabling a comparison to be made between matching simulations with different overall trajectories (i.e., different due to selection of different random seeds used in assigning initial atomic velocities). To verify that the selected temperature range was sufficient to enable sufficient conformational sampling, samples of the high-temperature replica structures for each of the simulated systems were examined for conformational disorder (i.e., resulting in a randomly structured peptide). For example, the LKα14 peptide, which typically maintains a helical conformation in solution at 298 K, was shown to adopt a random conformation when simulated at the 520 K temperature level.

There are a large variety of approaches to evaluating the state of convergence of an REMD simulation [41–48], and a consistent metric within all approaches is the convergence of specific system parameters of interest in the simulation. In our simulations, we were primarily concerned with structural features of the peptides and the surrounding solution as they interacted with the surface chemistries presented to them. Based on these structural analyses, including comparisons between the two independent sets of REMD simulations for each system, all REMD simulations appeared to have achieved convergence of all structural characteristics of interest within 3–5 ns of starting the simulations. Therefore, all simulations were continued through completion of 12 ns, with the last 6 ns of the simulation then used for final analyses of the sampled ensemble of equilibrated states.

2.3 Methods Used to Analyze REMD Results

The results from the REMD simulations, which were sampled every 1 ps, were analyzed to assess the development of secondary structure and the orientation of each peptide on each surface. Secondary structural analyses were performed in three ways. First, the phi (ϕ) and psi (ψ) dihedral angles of each amino acid residue of each peptide were determined for each sampled conformation over the full 12 ns of sampling to assess its secondary structural conformation as interpreted by the STRIDE [38] utility. Secondly, the ϕ and ψ angles from the last six nanoseconds of sampling (i.e., representing equilibrated structures) were then analyzed to calculate the relative free energies of each

conformation in order to quantitatively show the propensity for the amino acid residues to adopt the various conformational states. This was accomplished by dividing the ϕ/ψ dihedral angles of the representative Ramachandran plots into bins of 5° each and then counting the number of times each bin was sampled. The relative free energy (ΔG_r) of each dihedral conformational bin was then calculated by:

$$\Delta G_r = -RT \ln(N_i/N_T) \quad (1)$$

where N_i and N_T are the number of times each bin was sampled and the total number of samples for all bins, respectively, and R and T are the ideal gas constant and absolute temperature, respectively. Finally, the intermolecular distances separating the C_α carbons of the first and last L amino acid residues of the pair of LKβ7 peptides were used to assess the relative position and orientation of the LKβ7 peptides with respect to one another, thus characterizing the formation of parallel or antiparallel β-sheet structure on each surface. The conformation was labeled as a parallel β-sheet if the C-terminal carbons of both chains were within 8 Å of each other, and the N-terminal carbons of both chains were also within 8 Å. Likewise, the conformation was labeled as an antiparallel β-sheet if the C-terminal carbon of each chain was within 8 Å of the N-terminal carbon of the other. If neither criterion was met, the conformation was labeled as unstructured, or non-interactive. The distance of 8 Å between terminal carbons used as a threshold for categorizing the conformations as parallel/antiparallel or non-interactive was based on structural details of β-sheets [49] and used so that thermal fluctuations about a parallel or antiparallel arrangement would be included.

The adsorbed orientation of the peptides on each SAM surface was characterized by measuring the distance between each residue's side-chain terminus and the plane of the topmost carbon atoms of each SAM, which we define as the surface separation distance (SSD). Specifically, the leucine (L) side-chain terminus was defined as the geometrical center of the two methyl-group carbons at the end of its side chain and the lysine (K) side-chain terminus was defined as the nitrogen atom at the end of its side chain. Probability density (or frequency) plots were then generated for each amino acid residue as a function of its side-chain's SSD over the last 6 ns of REMD sampling to graphically show the tendency of the peptides to be oriented over each surface.

3 Results and Discussion

REMD does not represent a regular MD time sequence, but rather combines multiple parallel MD simulations of replicas of a system (40 replicas for each system in our case) that are simulated over a wide range of temperatures (298–520 K for our simulations) in order to rapidly cover the full conformational phase space of a molecular system. REMD then uses a Metropolis Monte Carlo-like process to construct a Boltzmann-weighted ensemble of states from the sampled phase space at each temperature level, with the 298 K level then used for our subsequent analyses. As noted in Sect. 2.2, we conducted 12 ns of REMD sampling for each of our systems in order to construct Boltzmann ensembles of conformational states. In order to provide evidence of convergence to an equilibrated ensemble of states, two things were necessary. First, it was necessary to ensure that the maximum temperature level used in our simulations (i.e., 520 K) was sufficiently high to cover the relevant peptide conformational space within a reasonable short period of time (i.e., fully folded to fully disordered states). As our most extreme case, preliminary studies showed that the LKα14 peptides transitioned from an α-helical conformation to fully disordered structures in both solution and on both surfaces within 1.0 ns, thus satisfying this condition. Secondly, the ensembles of states sampled from each pair of independent REMD simulations were analyzed to characterize each system's structural behavior, with these comparisons providing very similar distributions of states within 3–5 ns of REMD sampling, thus indicating convergence was reached within this level of REMD sampling time. The distribution of states from the last 6 ns of the full 12 ns of REMD sampling were then retained for analyses, with comparisons then made to the available experimental data. In making such comparisons, it is important to note that the simulated model SAM surfaces represent defect-free, idealized alkanethiol layers while experimental surfaces can be expected to contain various types of defects, such as grain boundaries, stepfaults, vacancies, and gauche rotations in the alkyl chains. Further studies are necessary to understand how such specific types of defects may influence the adsorption behavior of peptides on SAM surfaces.

3.1 Solution Structures of the LKβ7 and LKα14 Peptides

In solution (i.e., no SAM surface present), the pair of LKβ7 peptides did not associate with each other in a stable manner for any of the FFs used. Instead, the individual peptide strands exhibited variations in structure ranging from β-strand to random coil to slightly helical conformations. A comparison of the FFs based on the fraction of the REMD 298 K ensemble that adopted a random coil conformation shows distinct differences between the FFs (Fig. 1 in Supplementary Materials), with CHARMM22 and OPLS-AA exhibiting more random structure than AMBER94. Analyses of per-residue secondary structure

through the course of the REMD simulation (Fig. 3) provide an overview of the evolution of peptide structure. Figure 3 presents the structural evolution of the pair of LKβ7 peptides in solution for each FF over the full 12 ns of REMD simulation, with the associated Ramachadran-based relative free energy plots of the amino acid residue ϕ/ψ backbone dihedral angles for each FF over the last 6 ns of simulation. Using the CHARMM22 FF, these peptides primarily maintain their random coil conformation throughout the entire REMD simulation, with a small contribution from other motifs (Fig. 3a). The relative free energy plot of the ϕ/ψ backbone dihedral angles (Fig. 3d) shows that the CHARMM22 FF permits these peptides to explore a diverse range of backbone conformations with slightly greater propensity for the dihedral angle measurements to populate β-sheet regions of the plot. Using the AMBER94 FF, these peptides show a much greater tendency to form α-helical and turn conformations during the REMD simulation (Fig. 3b) compared to CHARMM22 (Fig. 3a). The Ramachandran plot (Fig. 3e) also indicates AMBER94 FF's tendency toward an α-helical backbone conformation. In contrast to CHARMM22 and AMBER94, the OPLS-AA FF caused the peptides to primarily explore both random coil and extended conformations (Fig. 3c),

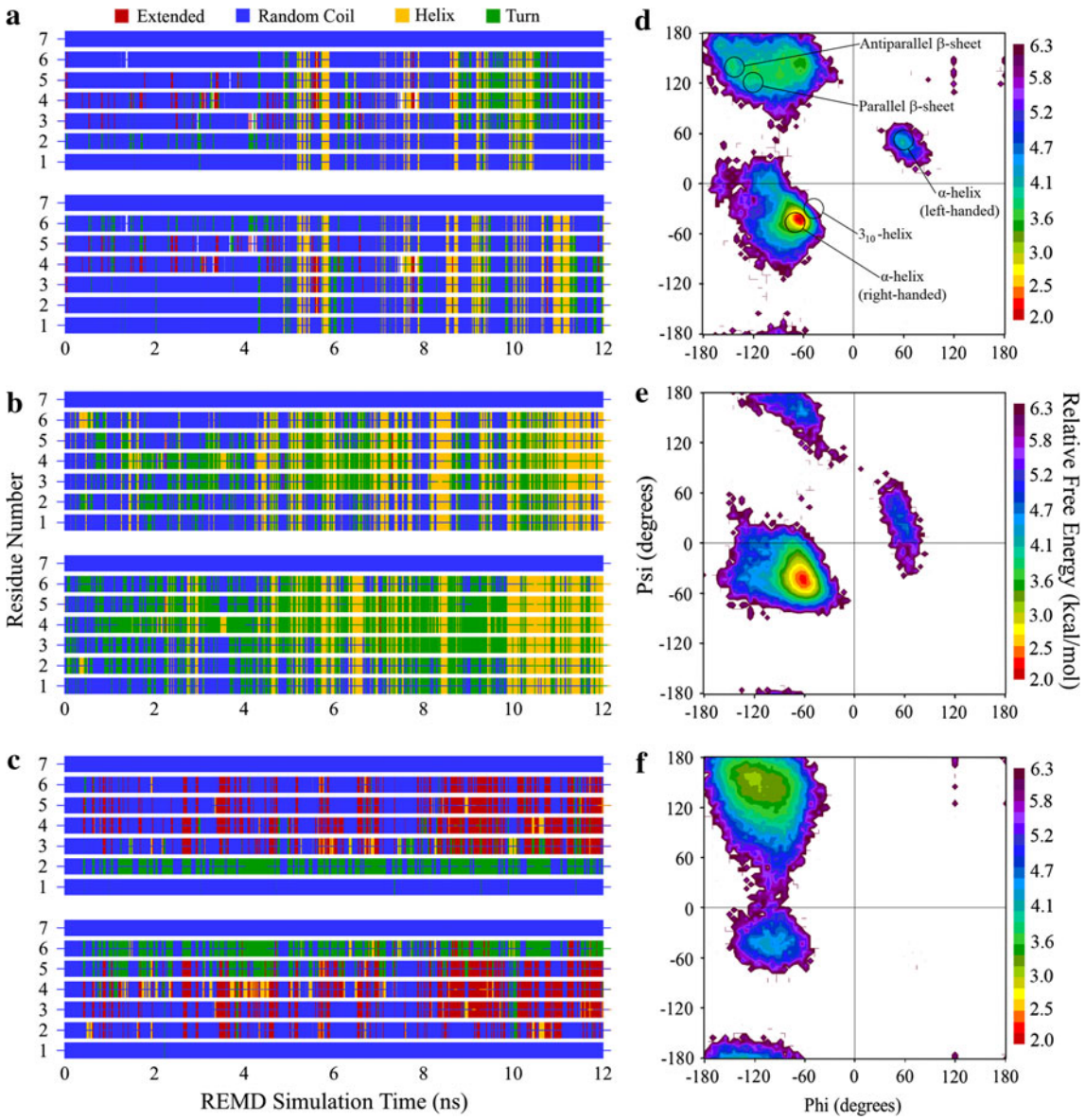

Fig. 3 Secondary structure for each amino acid residue through the entire REMD simulation for the pair of LKβ7 peptides in solution using **a** the CHARMM22 FF, **b** the AMBER94 FF, **c** the OPLS-AA FF, and Ramachandran plots of the relative free energy of different conformations obtained from the final 6 ns of REMD sampling for the pair of LKβ7 peptides in solution using **d** the CHARMM22 FF, **e** the AMBER94 FF, and **f** the OPLS-AA FF

with the Ramachandran plot showing a tendency toward a β-strand conformation (Fig. 3f), more similar to CHARMM22 (Fig. 3d) than AMBER94 (Fig. 3e).

Although very limited experimental data is available to assess which FF provides the most realistic results for a pair of LKβ7 peptides in solution, the results presented in Fig. 2 clearly show that these three FFs each predict substantially different conformational behavior in solution. Using circular dichroism spectropolarimetry (CD), DeGrado and Lear [7] observed that a dilute solution of LKβ7 peptides in Tris–HCl buffer showed approximately 50% β-sheet character, while Phillips and coworkers [8] have more recently noted that, in phosphate-buffered saline, predominantly random coil character is observed. Considering these observations when comparing the performance of these FFs, as depicted by the Ramachandran plot results shown in Fig. 3, suggests that the behavior represented by CHARMM22 and OPLS-AA FFs most closely match the experimentally observed behavior.

Results for the conformational behavior of the single LKα14 peptide in solution are presented in Fig. 4 with plots of amino acid residue secondary structural assignments over the full 12 ns and Ramachandran relative free energy plots for the last 6 ns. The solution conformation of the LKα14 peptide when using the CHARMM22 (Fig. 4a, d) and AMBER94 FFs (Fig. 4b, e) is predominantly α-helical, with the AMBER94 FF permitting more deviation from strictly α-helical conformations throughout the

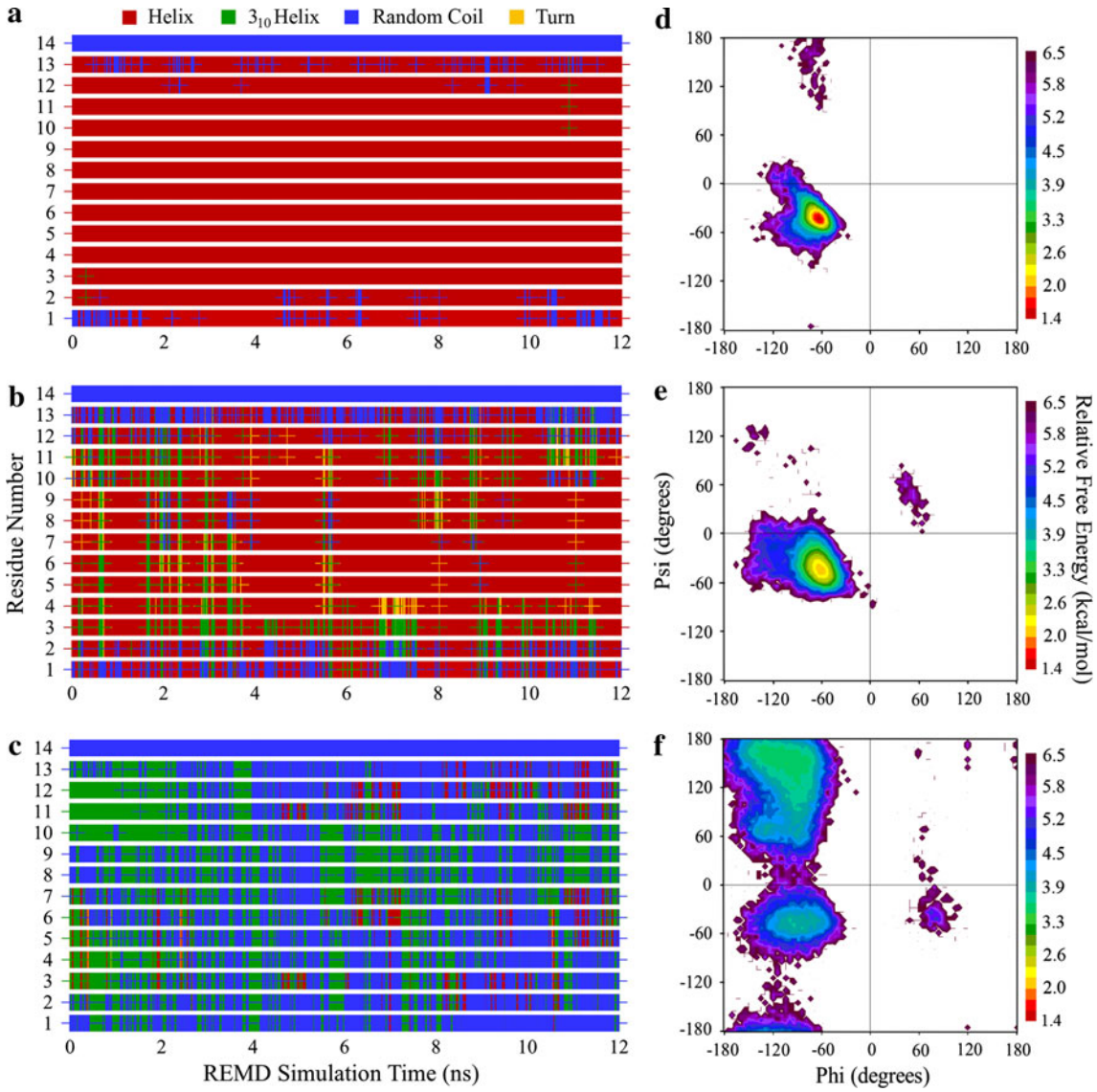

Fig. 4 Secondary structure for each amino acid residue through the entire REMD simulation for the LKα14 peptide in solution using **a** the CHARMM22 FF, **b** the AMBER94 FF, **c** the OPLS-AA FF, and Ramachandran plots of the relative free energy of different conformations obtained from the final 6 ns of REMD sampling for the LKα14 peptide in solution using **d** the CHARMM22 FF, **e** the AMBER94 FF, and **f** the OPLS-AA FF

entire REMD simulation. In contrast to CHARMM22 and AMBER94, the OPLS-AA FF presents the solution conformation of the LKα14 peptide as being mostly a random coil conformation (Fig. 4c), but with a substantial number of 3_{10}-helix conformations also appearing throughout the simulation. The relative free energies of conformations predicted by the OPLS-AA FF for this peptide cover a very wide range of values as evidenced by the broad energy wells spanning α-helical and β-strand ϕ/ψ backbone dihedral angle values (Fig. 4f).

Experimental results defining the structural behavior of the LKα14 peptide in solution obtained using CD indicate that it primarily maintains a stable α-helical conformation [7, 8], with the CHARMM22 and AMBER94 FFs thus being much more closely aligned with experimental results than the OPLS-AA FF. The fractional helicity predicted by each FF for specific LKα14 peptide residues is summarized in Fig. 2 (see Supplementary Materials).

3.2 The LKβ7 Pair Adsorbed to the CH_3-SAM

The simulation results for the structural behavior of the pair of LKβ7 peptides on the hydrophobic CH_3-SAM surface are presented in Fig. 5 with plots of amino acid residue

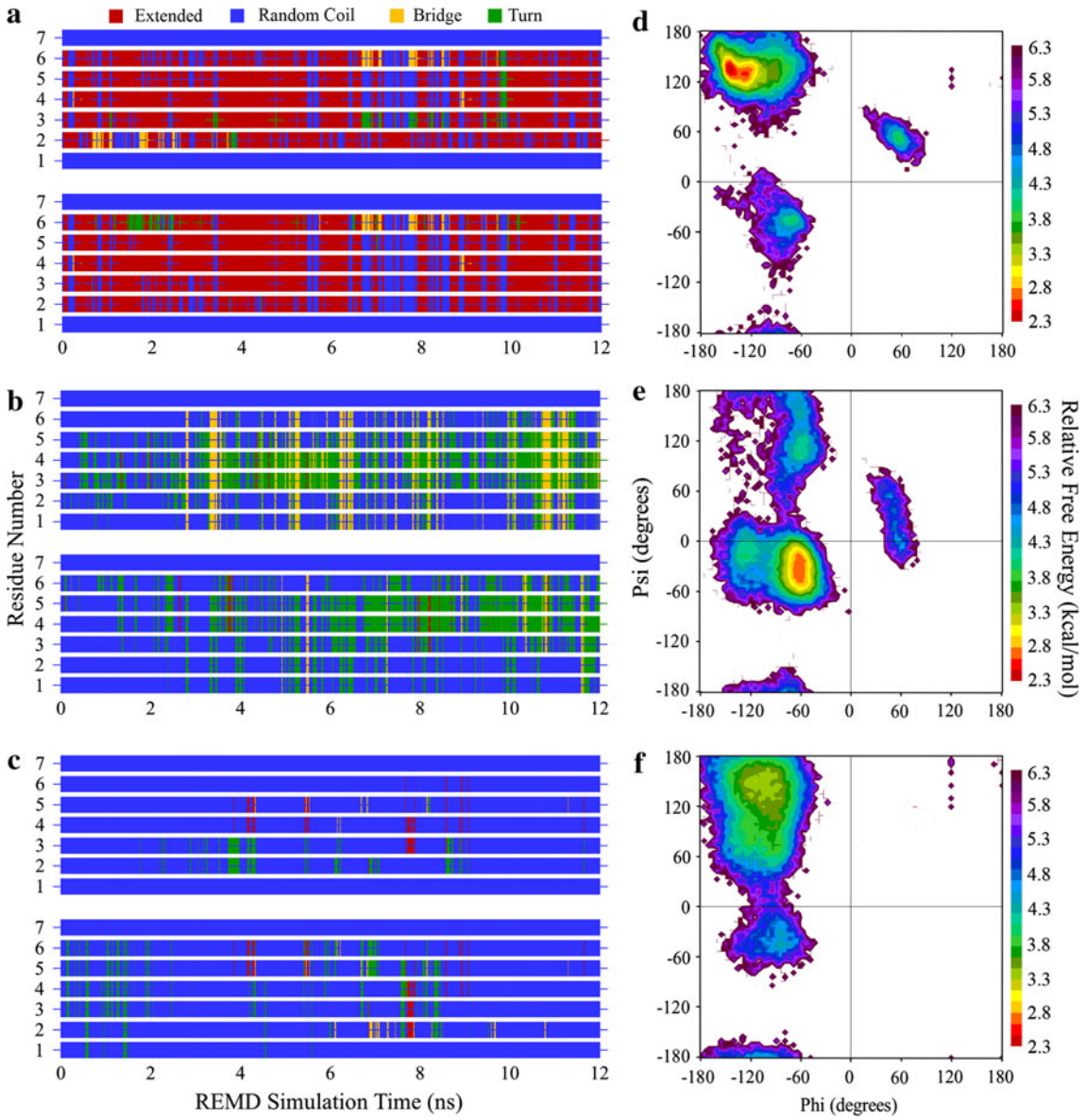

Fig. 5 Secondary structure for each amino acid residue through the entire REMD simulation for the LKβ7 pair of peptides adsorbed to the CH_3-SAM using **a** the CHARMM22 FF, **b** the AMBER94 FF, **c** the OPLS-AA FF, and Ramachandran plots of the relative free energy of different conformations obtained from the final 6 ns of REMD sampling for the LKβ7 pair of peptides adsorbed to the CH_3-SAM using **d** the CHARMM22 FF, **e** the AMBER94 FF, and **f** the OPLS-AA FF

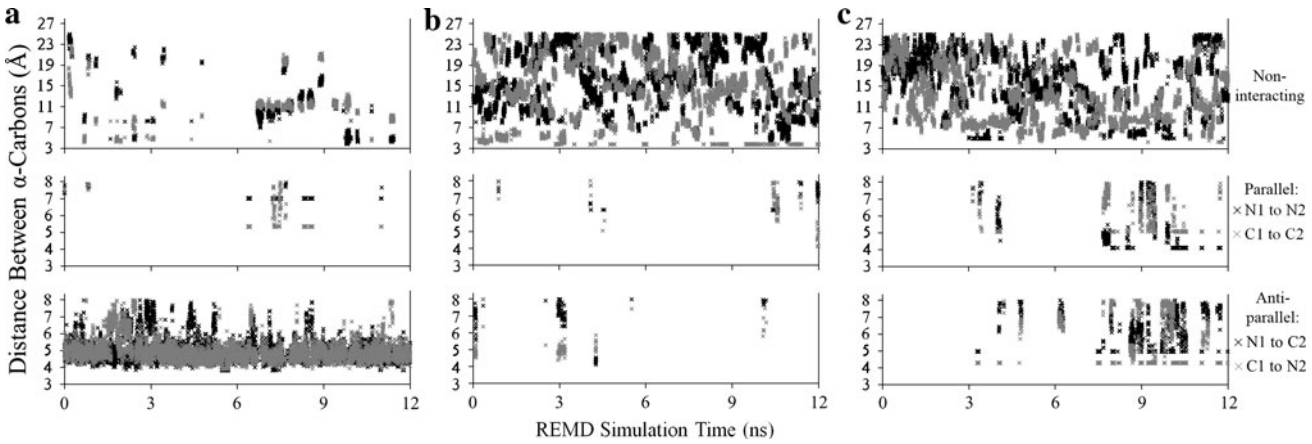

Fig. 6 Distances between terminal α-carbons (used to identify parallel and antiparallel conformations) for the pair of LKβ7 peptides adsorbed to the CH_3-SAM during the entire REMD simulation for **a** the CHARMM22 FF, **b** the AMBER94 FF, and **c** OPLS-AA FF

secondary structure assignments over the full 12 ns and Ramachandran relative free energy plots for the last 6 ns. When adsorbed to the CH_3-SAM, the CHARMM22 FF predicts that these peptides deviate from their random coil solution structure and consistently adopt an extended β-strand conformation (Fig. 5a). The backbone dihedral angles for this CHARMM22 system also reflect the same strong tendency (Fig. 5d), showing a distinct β-strand conformation with minor populations of both right- and left-handed helical conformations. In contrast to CHARMM22, the AMBER94 FF tended strongly toward an α-helical conformation (Fig. 5b, e) while the OPLS-AA FF sampled mostly random coil conformations along with a small amount of β-strand conformations (Fig. 5c, f). The fraction of extended β-strand conformations predicted by each FF for specific LKβ7 peptide residues is summarized in Fig. 3 (see Supplementary Materials), again showing the stronger preference of CHARMM22 for the β-strand structure when adsorbed.

Figure 6 presents the analyses of the association of the pair of LKβ7 peptides on the CH_3-SAM surface to form β-sheet structure. Only the CHARMM22 FF showed substantial development of β-sheet structure (Fig. 6a), with a strong bias toward the more energetically favorable antiparallel β-sheet. In contrast to this behavior, AMBER94 (Fig. 6b) exhibited predominantly non-interacting conformations, with OPLS-AA (Fig. 6c) indicated to mostly sample non-interacting structures but with a relatively small proportion of both parallel and antiparallel conformations. Comparison between the results shown in Fig. 6a for CHARMM22 with the extended-chain residue-by-residue structural assignments of Fig. 5a supports that the antiparallel configurations predicted in Fig. 6a for CHARMM22 are indeed representative of β-sheet structure. In contrast to this, Fig. 5c for OPLS-AA shows that the individual amino acids of both peptides were

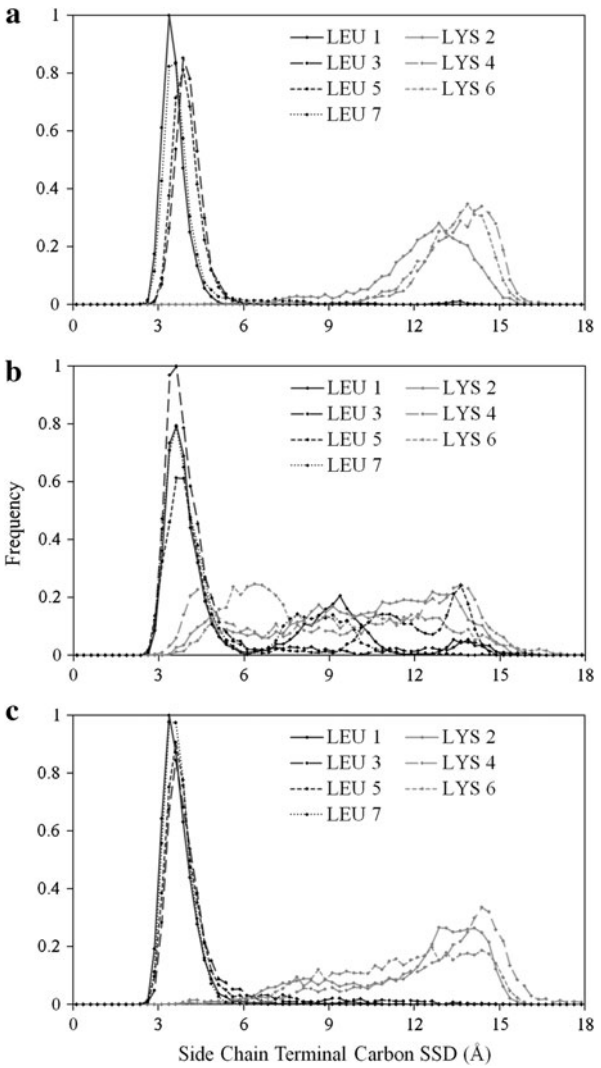

Fig. 7 Frequency distributions for amino acid side chain terminus surface separation distances (SSD) for the pair of LKβ7 peptides adsorbed to the CH_3-SAM during the last 6 ns of REMD sampling using **a** the CHARMM22 FF, **b** the AMBER94 FF, and **c** the OPLS-AA FF

predominantly configured in random coil structure, thus indicating that the apparent β-sheet structures assigned for OPLS-AA in Fig. 6c actually represent very irregular associations between the two LKβ7 strands as opposed to tightly conformed, stable β-sheet structures. Figure 2 illustrates an example of the conformational differences typically found for the stable antiparallel β-strand structure for the pair of LKβ7 peptides predicted by CHARMM22 (Fig. 2a) compared the much more unstructured association between the pair of LKβ7 peptides observed with OPLS-AA (Fig. 2b).

Measurements of the side-chain SSDs for the LKβ7 pair of peptides (Fig. 7) show that the arrangement of the L side chains relative to the surface of the CH_3-SAM is consistent between each of the three FFs, with the L side chains staying within a narrow range of distances from the surface (approximately 3–5 Å). The K side-chain SSD distributions, however, show significant differences, with the AMBER94 FF providing much more variability in the K side-chain SSDs (Fig. 7b) compared to CHARMM22 (Fig. 7a) and OPLS-AA (Fig. 7c), thus suggesting a broader range of orientations with AMBER94.

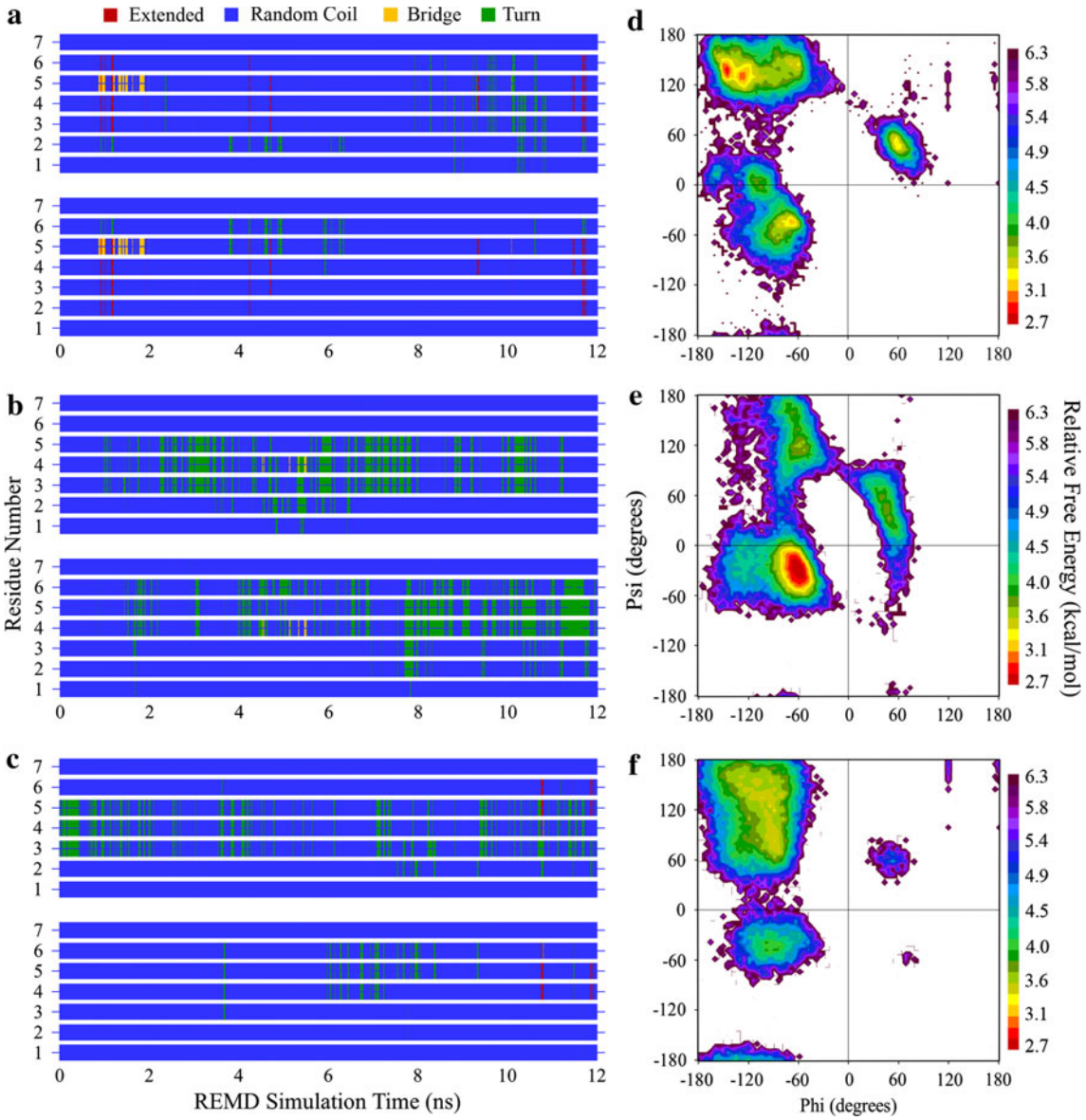

Fig. 8 Secondary structure for each amino acid residue through the entire REMD simulation for the pair of LKβ7 peptides adsorbed to the COOH-SAM using **a** the CHARMM22 FF, **b** the AMBER94 FF, **c** the OPLS-AA FF, and Ramachandran plots of the relative free energy of different conformations obtained from the final 6 ns of REMD sampling for the pair of LKβ7 peptides adsorbed to the COOH-SAM using **d** the CHARMM22 FF, **e** the AMBER94 FF, and **f** the OPLS-AA FF

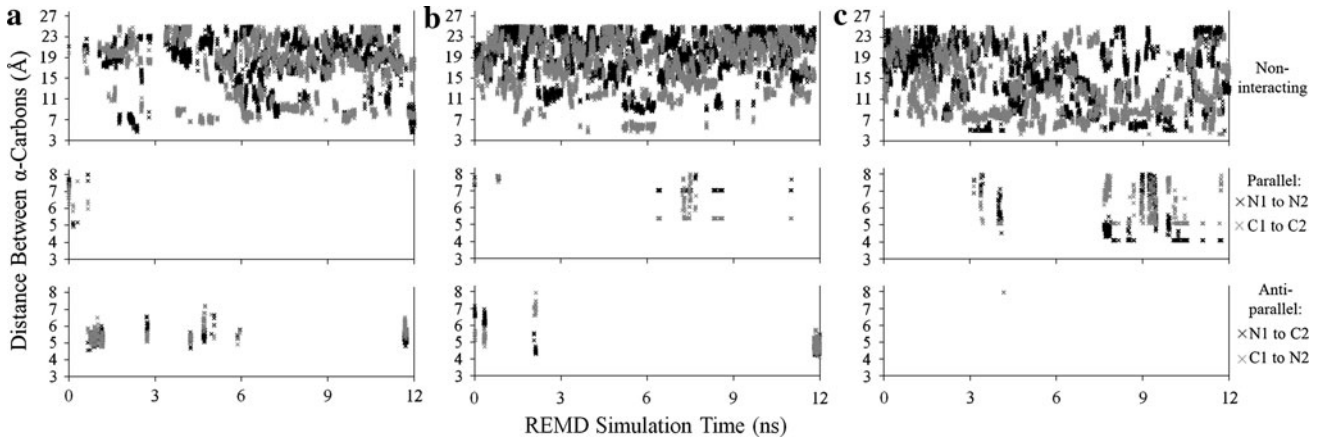

Fig. 9 Distances between terminal α-carbons (used to identify parallel and antiparallel conformations) for the pair of LKβ7 peptides adsorbed to the COOH-SAM during the entire REMD simulation for **a** the CHARMM22 FF, **b** AMBER94 FF, and **c** OPLS-AA FF

Experimentally, LKβ7 peptides have been shown to form stable β-sheet structures with the L amino acids adsorbed closer to the surface than the K amino acids on hydrophobic surfaces by DeGrado and Lear [7] (air–water interface and an apolar surface), by Phillips and coworkers [8] (hydrophobic polystyrene), and by Castner and coworkers [9, 11] (CH_3-SAMs). In addition, using infrared spectroscopy, DeGrado and Lear indicated that the β-sheet formed by the LKβ7 on an apolar surface occurred in an antiparallel structure, while using sum frequency generation (SFG), Castner and coworkers [11] indicated very distinct separation between the L and K amino acid residues on a CH_3-SAM surface using a 15 amino acid alternating LK peptide (LKβ15) as opposed to LKβ7. Thus, while all three FF were successful in correctly predicting the orientation of the LKβ7 peptides on a hydrophobic surface, CHARMM22 was the only FF that successfully predicted these peptides to form stable antiparallel β-sheet structures with tightly distributed orientations of the L and K residues.

3.3 The LKβ7 Pair Adsorbed to the COOH-SAM

The simulation results for the structural behavior of the pair of LKβ7 peptides on the negatively charged COOH-SAM surface are presented in Fig. 8 with plots of amino acid residue secondary structure assignments over the full 12 ns and Ramachandran relative free energy plots for the last 6 ns. When adsorbed to the COOH-SAM, the LKβ7 peptides do not adopt a particular secondary structure motif with any of the FFs used. Using any of the 3 FFs, there is little change from a random coil conformation through the entire REMD simulation. However, Ramachandran plots reveal different tendencies between these three FFs. The OPLS-AA results (Fig. 8f) show the greatest tendency toward a β-strand conformation with minor populations of

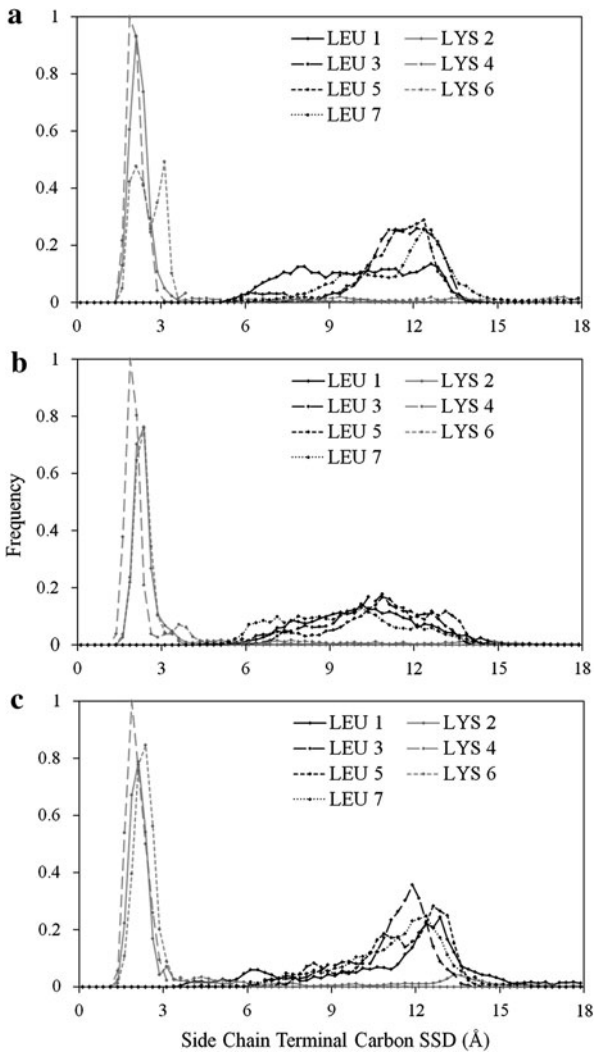

Fig. 10 Frequency distributions for amino acid side chain terminus surface separation distances (SSDs) for the pair of LKβ7 peptides adsorbed to the COOH-SAM during the last 6 ns of REMD sampling using **a** the CHARMM22 FF, **b** the AMBER94 FF, and **c** the OPLS-AA FF

helical conformations, CHARMM22 (Fig. 8d) showed about equal distribution between β-strand and helical conformations, while AMBER94 (Fig. 8e) shows a stronger propensity toward the formation of right-handed α-helix conformations. The fraction of random coil conformations predicted by each FF for specific LKβ7 peptide residues is summarized in Fig. 4 (see Supplementary Materials).

Distances between the terminal backbone carbons of the LKβ7 pair over the COOH-SAM (Fig. 9) indicate that there was little tendency to form either antiparallel or parallel β-sheet structures on the COOH-SAM surface with any of the three FFs. Despite the random conformational structure of the LKβ7 peptides on this surface, measurements of the side-chain SSDs reveal strong orientational ordering by each FF, with the positively charged lysine residues closer to the negatively charged COOH-SAM (Fig. 10). This is inverted, compared to the CH_3-SAM shown in Fig. 7. As shown in Fig. 10, the K side-chain SSDs fell within a narrow 2–3 Å range centered at approximately 2 Å from the surface for each FF, with each FF predicting a much wider distribution of the L amino acid residues.

Experimentally, DeGrado and Lear [7] reported that LKβ7 peptides formed stable antiparallel β-sheet structure on a hydrophilic quartz surface using CD and infrared

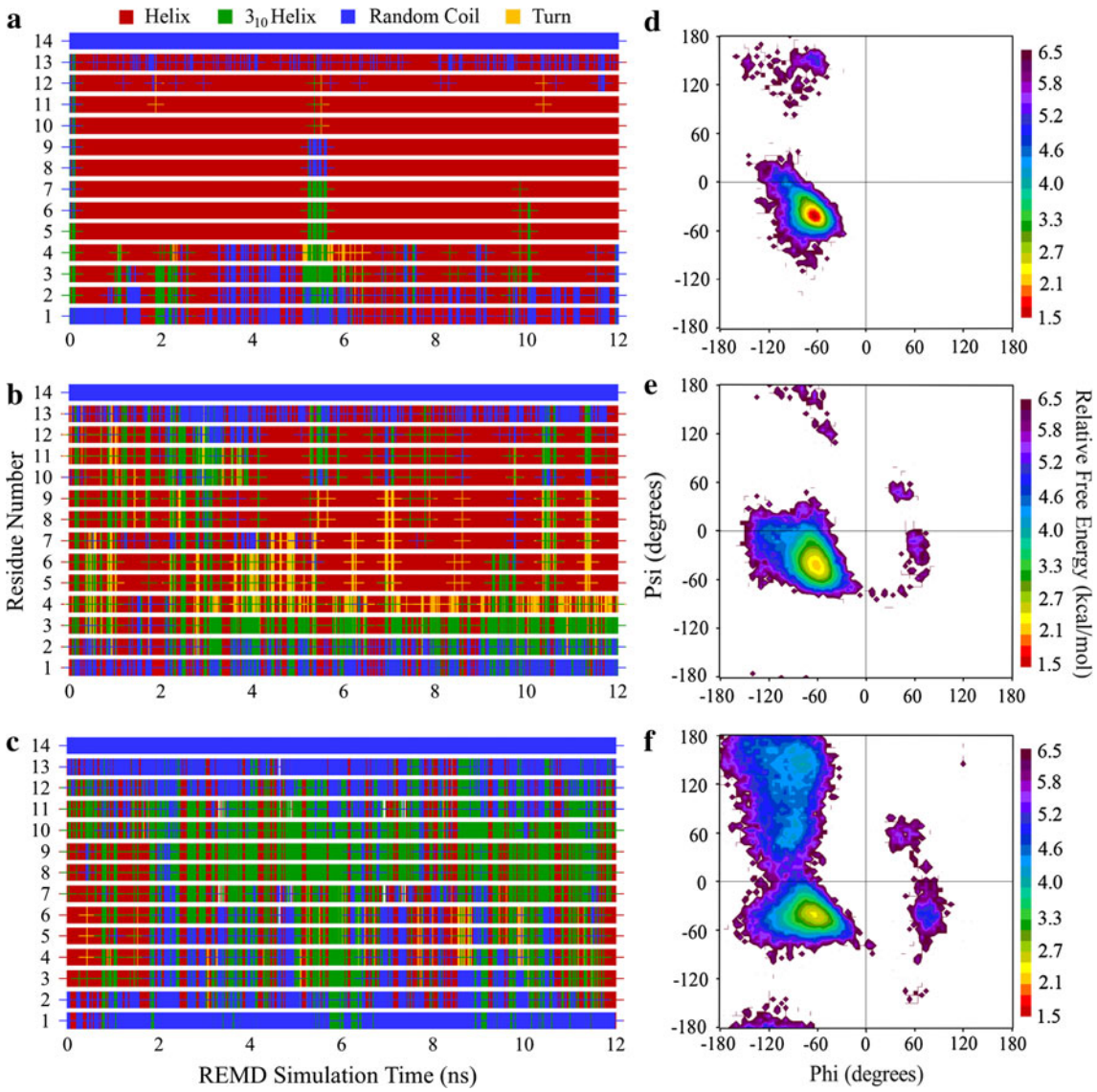

Fig. 11 Secondary structure for each amino acid residue through the entire REMD simulation for the LKα14 peptide adsorbed to the CH_3-SAM using **a** the CHARMM22 FF, **b** the AMBER94 FF, **c** the OPLS-AA FF, and Ramachandran plots of the relative free energy of different conformations obtained from the final 6 ns of REMD sampling for the LKα14 peptide adsorbed to the CH_3-SAM using **d** the CHARMM22 FF, **e** the AMBER94 FF, and **f** the OPLS-AA FF. The Ramachandran plots represent structures from the final 6 ns of REMD sampling, with α-helix structure simply designated as helix

spectroscopy, while both Castner and coworkers [9, 11] (LKβ15 peptides on COOH-SAM surface) and Phillips and coworkers [8] (LKβ7 peptides on hydrophilic silica) found that these LK peptides oriented with K residues adsorbed closer to the surface than the L residues using SFG, time-of-flight secondary ion mass spectrometry (ToF–SIMS), and near-edge X-ray absorption fine structure spectroscopy (NEXAFS), and using SFG, respectively.

Comparisons between our simulation results with the available experimental findings thus show that while all three FF were able to correctly predict the orientation of the LKβ7 peptides on the COOH-SAM surface, none of the FFs were able to predict the formation of stable β-sheet structure, thus indicating problems with force field parameterization for this type of system.

3.4 The LKα14 Peptide Adsorbed to the CH_3-SAM

The simulation results for the structural behavior of the single LKα14 peptide on the hydrophobic CH_3-SAM surface are presented in Fig. 11 with plots of amino acid residue secondary structure assignments over the full 12 ns and Ramachandran relative free energy plots for the last 6 ns. When adsorbed to the CH_3-SAM, the LKα14 peptide maintains a predominantly helical conformation with all three FFs, but the nature of the helical conformations varied amongst the different FFs. The CHARMM22 FF presents a strongly and consistently α-helical conformation throughout the simulation as evidenced by both secondary structure (Fig. 11a) and backbone dihedral angles (Fig. 11d). These results match the solution structure results for that FF (Fig. 4a, d), and most closely match experimental findings [9–11, 50]. As in the case of the LKβ7 peptides, it appears that the methyl-group parameters in CHARMM22 FF permit strong binding of the peptide with minimal disruption of the peptide's internal structure. The AMBER94 FF shows this peptide deviating from an α-helical conformation toward that of a 3_{10}-helix or a random coil (Fig. 11b) more often than is the case for the solution structures calculated using that FF (Fig. 4b). The Ramachandran relative free energy plot for this system also reflects a broader exploration of right-handed helical structures (Fig. 11e). The OPLS-AA FF results in conformations ranging from random coil to 3_{10}-helix and some α-helix (Fig. 11c). The backbone dihedral measurements for this varied population of structures reflect broadly right-handed helical character with much more exploration of extended strand conformations (Fig. 11f) compared with CHARMM22 and AMBER94. The fraction of α-helical conformations predicted by each FF for specific LKα14 peptide residues is summarized in Fig. 5 (see Supplementary Materials).

Because of its predominantly helical structure, the LKα14 peptide's side chains cannot be evenly segregated in the way that is possible for the LKβ7 peptides, so it is unavoidable for the side-chain SSDs of the LKα14 peptide to be less well ordered than they are for the LKβ7 peptides. However, when adsorbed to the CH_3-SAM, most of the LKα14 peptide's adsorbing L side chains are arranged so that their SSDs fall tightly within a 3 Å range, centered at approximately 4 Å from the SAM surface with all three FFs (Fig. 12), with the nonadsorbing K side chains distributed more widely. Overall, these results reflect a consistent preference for adsorption with the L residues oriented toward the surface, despite the differences in helical conformations amongst the different FFs used.

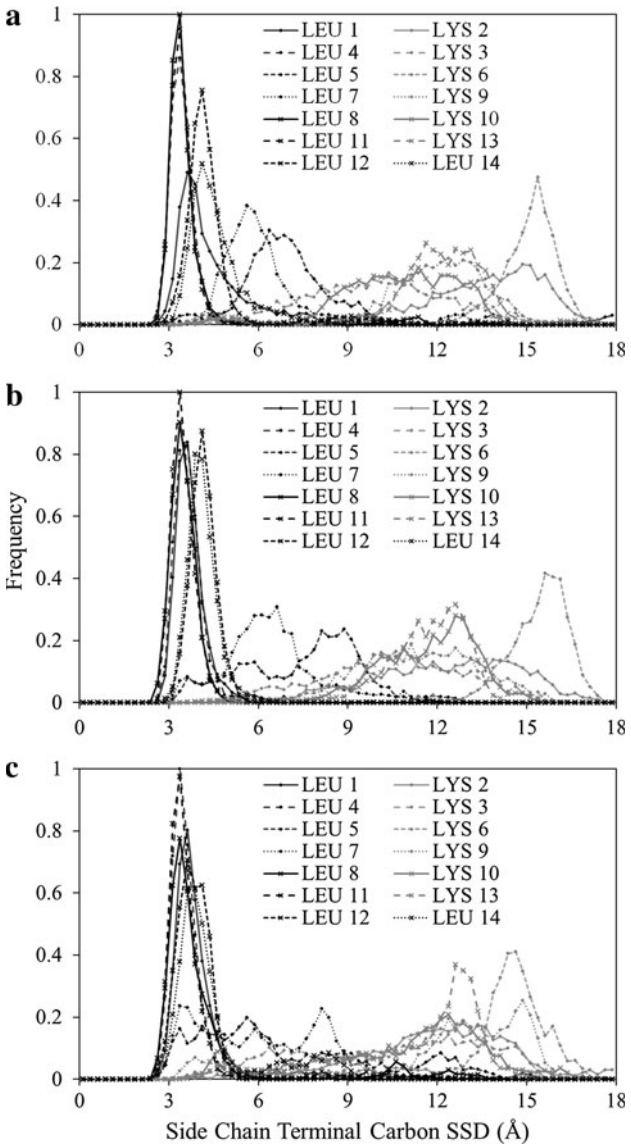

Fig. 12 Frequency distributions of amino acid side chain terminal carbon surface separation distances (SSDs) for the LKα14 peptide adsorbed to the CH_3-SAM during the last 6 ns of REMD sampling using **a** the CHARMM22 FF, **b** the AMBER94 FF, and **c** the OPLS-AA FF

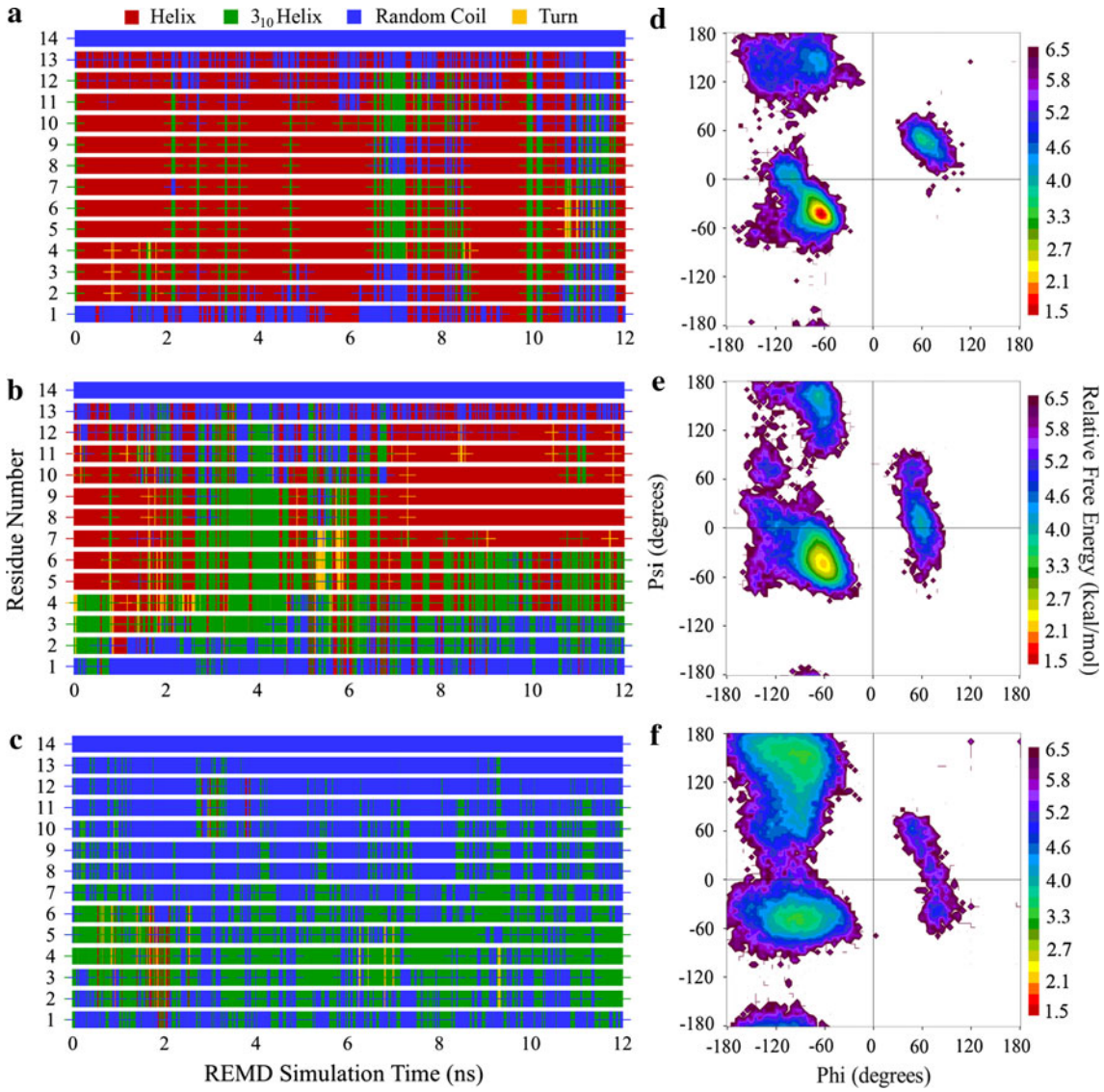

Fig. 13 Secondary structure for each amino acid residue through the entire REMD simulation for the LKα14 peptide adsorbed to the COOH-SAM using **a** the CHARMM22 FF, **b** the AMBER94 FF, **c** the OPLS-AA FF, and Ramachandran plots of the relative free energy of different conformations obtained from the final 6 ns of REMD sampling for the LKα14 peptide adsorbed to the COOH-SAM using **d** the CHARMM22 FF, **e** the AMBER94 FF, and **f** the OPLS-AA FF. The Ramachandran plots represent structures from the final 6 ns of REMD sampling, with α-helix structure simply designated as helix

Experimentally, DeGrado and Lear [7] reported LKα14 peptides to form stable helical structure on an apolar surface using CD and infrared spectroscopy, while Castner and coworkers [9, 11] (LKα14 on CH_3-SAM, using SFG, ToF–SIMS, and NEXAFS), and Phillips and coworkers [8] (LKα14 on hydrophobic polystyrene using SFG) reported the orientation of this peptide with the L residues oriented closer to the surface than the K residues. In addition, Castner and coworkers' ToF–SIMS results indicated much less separation between the L and K residues for this peptide compared to the LKβ15 peptide, which was presumed to reflect broader arrangement of the residues resulting from the helical structure of the LKα14 peptide.

Comparisons between our simulation results and the available experimental data thus show that while all three FFs are again able to correctly represent the orientation of the LKα14 peptide on the CH_3-SAM surface, only CHARMM22 and AMBER94 FFs provide close agreement with experimental findings regarding the stability of helical structure, with OPLS-AA not being able to adequately capture this type of structural behavior.

3.5 The LKα14 Peptide Adsorbed to the COOH-SAM

The simulation results for the structural behavior of the single LKα14 peptide on the negatively charged

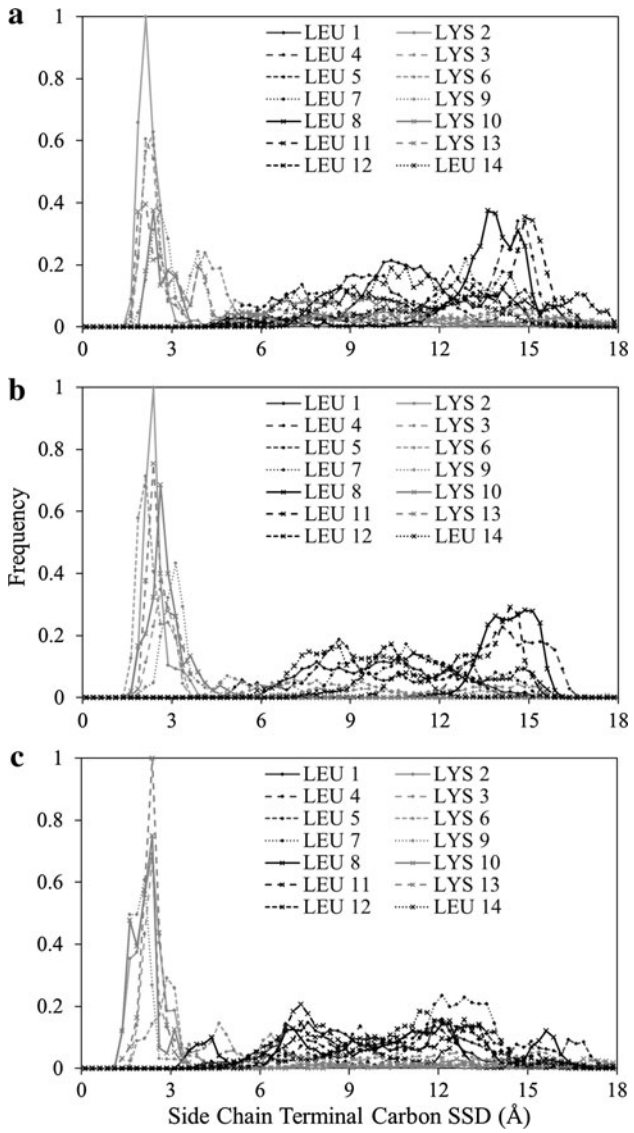

Fig. 14 Frequency distributions of amino acid side chain terminal carbon surface separation distances (SSDs) for the LKα14 peptide adsorbed to the COOH-SAM during the last 6 ns of REMD sampling using **a** the CHARMM22 FF, **b** the AMBER94 FF, and **c** the OPLS-AA FF

COOH-SAM surface are presented in Fig. 13 with plots of amino acid residue secondary structure assignments over the full 12 ns and Ramachandran relative free energy plots for the last 6 ns. The CHARMM22 FF shows substantial deviation from the predominantly α-helical conformation than was found for adsorption of this peptide to the CH_3-SAM (Fig. 11a). The backbone dihedral angles of the last 6 ns of sampling also show the conformations to be less strongly α-helical (Fig. 13d) than when adsorbed to the CH_3-SAM (Fig. 11d). Similar to CHARMM22, the AMBER94 FF also shows segments of this peptide deviating from an α-helical conformation toward that of a 3_{10}-helix in many instances during the REMD simulation (Fig. 13b), with the outer residues exhibiting more random-coil structure. Backbone dihedral angles explored using the AMBER94 FF (Fig. 13e) are quite similar to the distribution obtained with CHARMM22 (Fig. 13d), with a substantial amount of both β-sheet and left-handed helical conformations being present in the ensemble of sampled states. In distinct contrast to CHARMM22 and AMBER94 FFs, however, the OPLS-AA FF produced conformations ranging from a random coil to that of a 3_{10}-helix, with almost no α-helical conformations (Fig. 13c). The distribution of backbone dihedral angles with the OPLS-AA FF for this system (Fig. 13f) were similar to those for the LKβ7 peptides adsorbed to the COOH-SAM (Fig. 8f), but with many more helical conformations included. The fraction of α-helical conformation predicted by each FF for specific LKα14 peptide residues is summarized in Fig. 6 (see Supplementary Materials).

As shown in Fig. 14, the side-chain SSDs for the LKα14 peptide adsorbed to the COOH-SAM show an orientation that is inverted relative to adsorption to the CH_3-SAM. The adsorbing K side-chain SSDs fall within a 3 Å range, centered at approximately 2 Å from the SAM surface with all three FFs, with a very broad distribution of the L residues. This arrangement reflects a consistent preference among all three FFs for adsorption with the K residues positioned toward the surface, despite the substantial differences in helicity amongst the different FFs used.

Experimentally, DeGrado and Lear [7] reported that LKα14 peptides formed a stable helical structure on a hydrophilic quartz surface using CD and infrared spectroscopy. Castner and coworkers [9, 11] found evidence of the orientation of this peptide with the K residues more closely adsorbed to a COOH-SAM surface compared to the L residues using ToF–SIMS, SFG, and NEXAFS, but with the separation between the L and K residues being much less distinct than with the β-sheet forming LKβ15 peptides, which was again presumed to be due to the formation of helical vs. β-sheet structure.

Comparisons between the simulation and experimental results thus again show that each FF was able to represent the orientational behavior of this peptide on the COOH-SAM surface, with the CHARMM22 and AMBER94 FFs again predicting the formation of a much greater degree of helical structure in agreement with experimental results compared to the predominantly random structure predicted by OPLS-AA.

3.6 Force Field Comparisons

An overall comparison of FF performance relative to the available experimental results is presented in Table 1. Each FF is evaluated for its consistency with the experimental observations. From these comparisons, it can be seen that

Table 1 A qualitative comparison of FF performance, comparing experimentally observed behavior

Performance consideration (experimental finding)	Estimation of performance		
	CHARMM22	AMBER94	OPLS-AA
LKβ7s in solution adopt a random coil conformation	+	−	+
LKβ7s interact with (adsorb to) the CH_3-SAM	++	++	++
LKβ7s form β-strands when adsorbed to the CH_3-SAM	++	−−	−
LKβ7s form β-sheet when adsorbed to the CH_3-SAM	++	−−	−
LKβ7s oriented LEU-down when adsorbed to the CH_3-SAM	++	+	++
LKβ7s interact with (adsorbed to) the COOH-SAM	++	++	++
LKβ7s form β-strands in the presence of the COOH-SAM	+	−−	−
LKβ7s form β-sheet when adsorbed to the COOH-SAM	−−	−−	−−
LKα14 in solution remains α-helical	++	++	−
LKα14s interact with (adsorb to) the CH_3-SAM surface	++	++	++
LKα14 remains α-helical when adsorbed to CH_3-SAM	++	+	−
LKα14 oriented LEU-down when adsorbed to CH_3-SAM	++	++	++
LKα14s interact with (adsorbed to) the COOH-SAM surface	++	++	++
LKα14 remains α-helical when adsorbed to COOH-SAM	+	+	−
LKα14 oriented LYS-down when adsorbed to COOH-SAM	++	++	++

+, Adherence to experimentally observed behavior; −, deviation from experimentally observed behavior

the CHARMM22 FF was most successful at replicating the experimentally observed behavior overall. The AMBER94 FF performed almost equally well in simulations involving the LKα14 peptide, but the AMBER94 performance for the LKβ7 systems was inconsistent with particularly poor performance in treating the structure of the LKβ7 peptides when they were adsorbed to either surface. The OPLS-AA FF performance was generally not as good as that of either the CHARMM22 or AMBER94 FFs.

Differences in the simulated adsorption behavior of the LK peptides on the represented SAM surfaces obtained with these three different force fields can be considered to be primarily due to differences in the values of their nonbonded parameters, which govern the complex competitive interactions between the peptide, water, and ions in solution for the functional groups of the SAM surfaces. The individual nonbonded parameters of each FF are provided in the Supplementary Materials section (Tables 1–6), along with a more detailed discussion of how the differing parameter values may affect adsorption behavior. However, cooperative and nonlinear effects of the force field parameters and the molecular behavior of these systems make it very difficult to clearly associate differences in parameterization between these three FFs with differences in simulated adsorption behavior. Further details on the methods and results from this study are provided in G. Collier's doctoral dissertation [51].

4 Conclusions

Our simulations of the interactions between the structured LK peptides and functionalized SAM surfaces provide a means of evaluating the applicability of the CHARMM22, AMBER94, and OPLS-AA FFs to interfacial systems. Of course, the differences, or strengths and weaknesses, amongst these FFs are difficult to fully identify from a limited number of model system simulations and given the limited experimental data, but some significant trends are noted. Overall, the CHARMM22 FF most closely matched experimental results for these simulations. The conformations of the pair of LKβ7 peptides and the single LKα14 peptide on each surface were both stable and most accurate when using the CHARMM22 FF based on comparison with the available experimental data. Most notably, the CHARMM22 FF was the only FF with which the pair of LKβ7 peptides adopted a stable antiparallel β-sheet configuration over the CH_3-SAM surface, which occurred in the adsorbed state but not in solution.

The results obtained using the AMBER FF agreed with experimental observations almost as well as the CHARMM22 FF, but in all simulations the AMBER FF generated significantly more variability in all structural and orientation measurements. The results obtained using the OPLS-AA FF deviated significantly from experimental results. In all simulations with the OPLS-AA FF, there was a pronounced tendency for the peptides to adopt a random coil configuration.

Molecular simulations using empirical force field methods have the inherent capability to provide a very powerful tool to study and understand the atomic level interactions that mediate peptide and protein adsorption behavior. While firm conclusions cannot be made regarding the extension of these results to other specific peptides and proteins, the results of our simulations do suggest that the CHARMM22 FF should generally predict more reliable

conformational behavior of adsorbed peptides and proteins on these types of surface structures and chemistries than that provided by the AMBER94 and OPLS-AA FFs. As clearly shown from the results of this present study, different empirical force fields can predict substantial differences in peptide adsorption behavior, and even their conformational behavior in solution. These results underscore the need for synergistic, closely matched experimental and computational studies that can be used to quantitatively assess the ability of a selected force field to adequately represent peptide-surface interactions so that force field performance can be properly evaluated and validated for selected applications. Only then can the full potential of molecular simulation methods be realized to accurately predict protein adsorption behavior to material surfaces.

Acknowledgments This work was funded under NIH Grant No. R01 GM074511 with additional funding support provided by NIH Grant Nos. R01 EB006163 and P41 EB001046-03. Computational support for this research was provided by the National Science Foundation through TeraGrid resources provided by the QueenBee and Abe clusters under grant number TG-BCS080004 N. The authors thank the Castner group at the University of Washington, Seattle, WA for their collaboration and helpful discussions regarding their experimental studies on LK peptide adsorption behavior. The authors also thank Dr. J. Barr von Oehsen and Ms. Corey Ferrier for support of the Palmetto Cluster computational resources at Clemson University.

References

1. Leach AR (2001) Molecular modelling: Principles and applications, 2nd edn. Pearson Education Limited, Harlow
2. Oostenbrink C, Villa A, Mark AE, Van Gunsteren WF (2004) J Comput Chem 25:1656–1676
3. van Gunsteren W, Billeter SR, Eising AA, Hunenberger P, Kruger P, Mark A, Scott WRP, Tironi I (1996) Biomolecular simulation: the GROMOS96 manual and user guide. Verlag der Fachvereine Hochschulverlag AG an der ETH Zurich and BIOMOS, Groningen
4. MacKerell AD Jr, Bashford D, Bellott M, Dunbrack RL, Evanseck JD, Field MJ, Fischer S, Gao J, Guo H, Ha S, Joseph-McCarthy D, Kuchnir L, Kuczera K, Lau FTK, Mattos C, Michnick S, Ngo T, Nguyen DT, Prodhom B, Reiher W E III, Roux B, Schlenkrich M, Smith JC, Stote R, Straub J, Watanabe M, Wiorkiewicz-Kuczera J, Yin D, Karplus M (1998) J Phys Chem B 102:3586–3616
5. Cornell WD, Cieplak P, Bayly CI, Gould IR, Merz KM, Ferguson DM, Spellmeyer DC, Fox T, Caldwell JW, Kollman PA (1995) J Am Chem Soc 117:5179–5197
6. Jorgensen WL, Maxwell DS, Tirado-Rives J (1996) J Am Chem Soc 118:11225–11236
7. DeGrado WF, Lear JD (1985) J Am Chem Soc 107:7684–7689
8. Phillips DC, York RL, Mermut O, McCrea KR, Ward RS, Somorjai GA (2007) J Phys Chem C 111:255–261
9. Apte JS, Collier G, Latour RA, Gamble LJ, Castner DG (2010) Langmuir 26:3423–3432
10. Weidner T, Samuel NT, McCrea K, Gamble LJ, Ward RS, Castner DG (2010) Biointerphases 5:9–16
11. Weidner T, Apte JS, Gamble LJ, Castner DG (2010) Langmuir 26:3433–3440
12. Weidner T, Breen NF, Li K, Drobny GP, Castner DG (2010) Proc Natl Acad Sci USA 107:13288–13293
13. Mackerell AD, Feig M, Brooks CL (2004) J Comput Chem 25:1400–1415
14. Vericat C, Vela ME, Benitez GA, Gago JAM, Torrelles X, Salvarezza RC (2006) J Phys Condens Mater 18:R867–R900
15. Grunze M (1993) Phys Scripta 1993:711–717
16. Latour RA, Rini CJ (2002) J Biomed Mater Res 60:564–577
17. Latour RA, Hench LL (2002) Biomaterials 23:4633–4648
18. Agashe M, Raut V, Stuart SJ, Latour RA (2005) Langmuir 21:1103–1117
19. Raut VP, Agashe MA, Stuart SJ, Latour RA (2005) Langmuir 21:1629–1639
20. Basalyga DM, Latour RA Jr (2003) J Biomed Mater Res A 64:120–130
21. Collier G, Vellore NA, Stuart SJ, Latour RA (2009) Biointerphases 4:57–64
22. Fears KP, Creager SE, Latour RA (2008) Langmuir 24:837–843
23. Tobias DJ, Mar W, Blasie JK, Klein ML (1996) Biophys J 71:2933–2941
24. Nordgren CE, Tobias DJ, Klein ML, Blasie JK (2002) Biophys J 83:2906–2917
25. Zhou J, Zheng J, Jiang S (2004) J Phys Chem B 108:17418–17424
26. Mar W, Klein ML (1994) Langmuir 10:188–196
27. Hautman J, Bareman JP, Mar W, Klein ML (1991) J Chem Soc Faraday Trans 87:2031–2037
28. Zheng J, Li L, Chen S, Jiang S (2004) Langmuir 20:8931–8938
29. Brooks BR, Bruccoleri RE, Olafson BD, States DJ, Swaminathan S, Karplus M (1983) J Comput Chem 4:187–217
30. Darden TA, York D, Pedersen LG (1993) J Chem Phys 98:10089–10092
31. Feller SE, Pastor RW, Rojnuckarin A, Bogusz S, Brooks BR (1996) J Phys Chem 100:17011–17020
32. Swope WC, Andersen HC, Berens PH, Wilson KR (1982) J Chem Phys 76:637–649
33. Evans DJ, Holian BL (1985) J Chem Phys 83:4069–4074
34. Ryckaert J, Ciccotti G, Berendsen HJC (1977) J Comput Phys 23:327–341
35. Yancey JA, Vellore NA, Collier G, Stuart SJ, Latour RA (2010) Biointerphases 5:85–95
36. Sugita Y, Okamoto Y (1999) Chem Phys Lett 314:141–151
37. Feig M, Karanicolas J, Brooks CL (2004) J Mol Graph Model 22:377–395
38. Frishman D, Argos P (1995) Proteins 23:566–579
39. Humphrey W, Dalke A, Schulten K (1996) J Mol Graph 14:33–38
40. Pettersen EF, Goddard TD, Huang CC, Couch GS, Greenblatt DM, Meng EC, Ferrin TE (2004) J Comput Chem 25:1605–1612
41. Simmerling C, Strockbine B, Roitberg AE (2002) J Am Chem Soc 124:11258–11259
42. Kameda T, Takada S (2006) P Natl Acad Sci USA 103:17765–17770
43. Jas GS, Kuczera K (2004) Biophys J 87:3786–3798
44. Zhang J, Li W, Wang J, Qin M, Wang W (2008) Proteins 72:1038–1047
45. Zhang W, Wu C, Duan Y (2005) Convergence of replica exchange molecular dynamics. J Chem Phys 123:154105-1–154105-9

46. Ruscio JZ, Fawzi NL, Head-Gordon T (2010) J Comput Chem 31:620–627
47. Grossfield A, Feller SE, Pitman MC (2007) Proteins 67:31–40
48. Faraldo-Gómez JD, Forrest LR, Baaden M, Bond PJ, Domene C, Patargias G, Cuthbertson J, Sansom MSP (2004) Proteins 57:783–791
49. Branden C, Tooze J (1999) Introduction to protein structure, 2nd edn. Garland Publishing, New York
50. Breen NF, Weidner T, Li K, Castner DG, Drobny GP (2009) J Am Chem Soc 131:14148–14149
51. Collier G (2011) PhD dissertation, Clemson University